Cascaded Incremental Nonlinear Dynamic Inversion Control for MAV Disturbance Rejection

Ewoud J.J. Smeur, Guido C.H.E. de Croon and Qiping Chu

arXiv:1701.07254v1 [cs.RO] 25 Jan 2017

***Abstract*—Micro Aerial Vehicles (MAVs) are limited in their operation outdoors near obstacles by their ability to withstand wind gusts. Currently widespread position control methods such as Proportional Integral Derivative control do not perform well under the influence of gusts. Incremental Nonlinear Dynamic Inversion (INDI) is a sensor-based control technique that can control nonlinear systems subject to disturbances. It was developed for the attitude control of manned aircraft or MAVs. In this paper we generalize this method to the outer loop control of MAVs under severe gust loads. Significant improvements over a traditional Proportional Integral Derivative (PID) controller are demonstrated in an experiment where the quadrotor flies in and out of a windtunnel exhaust at 10 m/s. The control method does not rely on frequent position updates, as is demonstrated in an outside experiment using a standard GPS module. Finally, we investigate the effect of using a linearization to calculate thrust vector increments, compared to a nonlinear calculation. The method requires little modeling and is computationally efficient.**

***Index Terms*—Quadrocopter, incremental control, INDI, disturbance rejection, wind gusts.**

I. Introduction

MICRO Aerial Vehicles (MAV) have the potential to perform many useful tasks, such as search and rescue [1], package delivery [2], aerial imaging [3], etc. In many of these applications, usage of autonomous MAVs can potentially result in significant cost reduction as compared to current practice. But in order to perform these tasks in an outdoor environment, the vehicles need to be able to control their position under the influence of wind gusts. This is especially true when flying close to obstacles, as a position error due to a wind gust might result in a collision.

Outdoor MAV missions can encounter significant gusts due to atmospheric turbulence [4]. Moreover, Orr et al. [5] showed that even a uniform wind can create a very non-uniform wind field in an urban environment. Computational fluid dynamics calculations showed that with a free stream velocity of 4.6 m/s, flow velocities ranging from 0 to 7.6 m/s are found around buildings. An MAV flying amidst these buildings can be expected to be subject to up to 7.6 m/s gusts. If such an MAV were to enter a building through an open window in case of a search and rescue mission, it would also experience a sudden change in wind speed. This scenario is especially challenging due to the confined space of a typical room. And even indoors, an MAV can be subject to aerodynamic disturbances, for instance caused by its own propeller backwash near walls [6].

The authors are with the Department of Aerospace Engineering, Delft University of Technology, 2629HS Delft, The Netherlands e-mail: e.j.j.smeur@tudelft.nl.

Clearly, a controller that is able to counteract wind gust disturbances would be of great value. Currently widespread position control methods such as Proportional Integral Derivative control (PID), which are used even for aggressive control [7], do not perform well under the influence of gusts. PID gust rejection properties scale with magnitude of the gains, which is often limited by the GPS update frequency in outdoor scenarios. Moreover, the integrator term is generally slow in compensating persistent wind disturbances.

To cope with wind gusts, a solution could be to use onboard Pitot tubes to measure the relative velocity of the MAV with respect to the wind. The difference with the ground speed measured by a GPS module can provide an estimate of the local wind [8]. As disturbances may come from all directions, a minimum of six Pitot tubes would be necessary (two for each axis, as a Pitot tube can not measure negative airspeed). Alternatively, Mohamed et al. [9] used multiple multi-probe sensors to obtain flow pitch angle and velocity. Adding such an amount of extra sensors will increase the system complexity and cost. Furthermore, airspeed sensors are typically not reliable at low airspeeds.

Instead of using sensors, one could use a model of the MAV to estimate the wind velocity [10]. Waslander and Wang [11] used an extensive aerodynamic model to estimate wind velocities, with good results in simulation. The downside of this approach is that it requires a lot of parameters, which might even require windtunnel tests as is done by Schiano et al. [12] and Tomic et al. [13]. If the model does not represent reality well enough due to modeling errors or airframe changes, the gust disturbance rejection performance will degrade.

In this paper, we introduce a gust resistant controller through generalization of Incremental Nonlinear Dynamic Inversion (INDI) to the outer loop control. The idea is that both disturbances as well as control forces are measured by the accelerometer. This means that a desired acceleration can be achieved by incrementing the previous control input based on the difference between desired and measured acceleration. We show how to deal with filtering of noisy acceleration measurements, and how this integrates with the INDI attitude controller we developed previously [14]. We will also demonstrate that the disturbance rejection capabilities of the INDI inner loop extend to the outer loop control.

The controller is implemented on a Parrot Bebop quadrotor running the Paparazzi open source autopilot software[1] [15], [16]. Windtunnel experiments show that the quadrotor can

[1]We have incorporated the INDI control method in Paparazzi, allowing others to easily experiment with it as well.

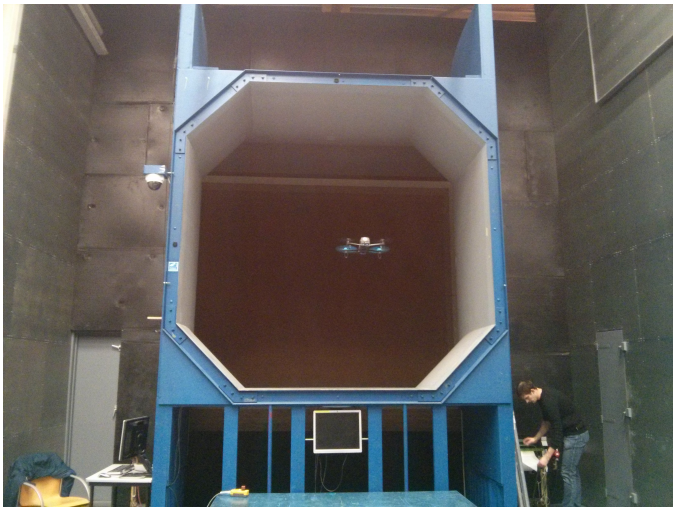

Fig. 1. The quadrotor in front of the windtunnel during one of the experiments.

enter and leave the 10 m/s windtunnel flow with only 20 cm maximum position deviation on average. A controller that uses a gain on the integrated error instead of the incremental controller, suffered 146 cm maximum position deviation upon entering and leaving the windtunnel on average. A picture of the experiment is shown in Figure 1.

This paper is an extension to the work presented at the Intelligent Robots and Systems conference [17]. Differences include: (1) the use of a large open jet windtunnel as a more accurate and more powerful disturbance than the fan used previously. (2) Incorporation of the propeller thrust curve to calculate the total thrust of the drone. (3) An outdoors experiment based on GPS positioning, to demonstrate the performance in a realistic scenario. (4) The addition of a nonlinear method to calculate thrust vector increments.

A. Related Work

Hoffmann et al. [18] developed an altitude controller that utilizes the vertical acceleration measurement. However, they fed the acceleration back, multiplied with a gain, without utilizing the physical relation between thrust and acceleration. In a different paper, they state that their PID position control implementation has little ability to reject disturbances from wind and translational velocity effects [19]. A vertical controller using the INDI principle was developed for a traditional helicopter in simulation by Simplicio et al. [20]. Only very limited sensor noise was taken into account, which did not require any filtering. Also, in both of these papers, by separating the vertical axis from the lateral axes, coupling can be expected. We show that by inverting the control effectiveness for all axes, accelerations in each of these axes can be controlled.

Wang et al.[21] applied an acceleration feedback dynamic inversion approach to all axes of a quadrotor, and demonstrated accurate trajectory tracking capabilities. They mentioned robustness against disturbances, but did not analyze or demonstrate the controller response against disturbances. Also, the effects of accelerometer noise or filtering are not discussed. Additional differences with the work presented here are that we do not have a need for a reference model or command filtering, and that their approach is not incremental. This means that if a certain control input does not completely resolve a measured acceleration error (due to input modeling errors or uncertainties), the error will persist. In an incremental scheme the input can be incremented again to resolve angular acceleration errors.

II. Incremental Nonlinear Dynamic Inversion for Attitude Control

An extended analysis of INDI for attitude control of MAVs is provided in previous work [14]. For completeness, an overview of the developed attitude controller, along with some new additions, is presented in this section. Consider the quadrotor shown in Figure 2. The distance from the center of gravity to each of the rotors along the X axis is given by l and along the Y axis by b.

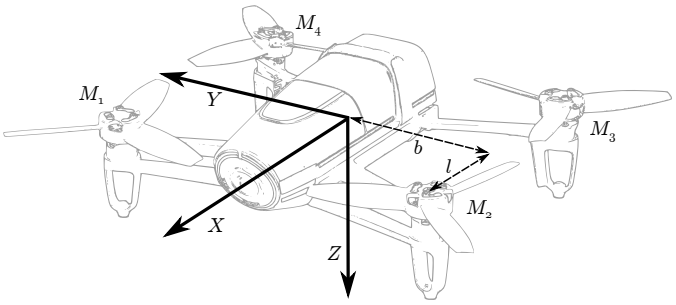

Fig. 2. The Bebop Quadcopter used in the experiments with body axis definitions.

We define that $\boldsymbol{\Omega}$ is the angular rate vector of the vehicle and the angular rates of the propellers around the body Z axis are described with the vector $\boldsymbol{\omega}$. We also define that T is the thrust provided by all four rotors. Consider Eq. 1, which gives an expression for the angular acceleration and the thrust:

$$\begin{bmatrix} \dot{\boldsymbol{\Omega}} \\ T \end{bmatrix} = \boldsymbol{F}(\boldsymbol{\Omega}, \boldsymbol{v}) + \boldsymbol{G}(\boldsymbol{\omega}, \dot{\boldsymbol{\omega}}) \tag{1}$$

Here, $\boldsymbol{F}(\boldsymbol{\Omega}, \boldsymbol{v})$ is the function that describes the vehicle moments as a function of the angular rates and velocity. $\boldsymbol{G}(\boldsymbol{\omega}, \dot{\boldsymbol{\omega}})$ is the function that maps the input and the derivative of the input to the angular acceleration and thrust. Note that the thrust force only depends on the rotational rate of the rotors, and so, the fourth row of the $\boldsymbol{F}(\boldsymbol{\Omega}, \boldsymbol{v})$ matrix is zero. Now we can apply a first order Taylor expansion:

$$\begin{aligned} \begin{bmatrix} \dot{\boldsymbol{\Omega}} \\ T \end{bmatrix} = \; & \boldsymbol{F}(\boldsymbol{\Omega}_0, \boldsymbol{v}_0) + \boldsymbol{G}(\boldsymbol{\omega}_0, \dot{\boldsymbol{\omega}}_0) \\ & + \tfrac{\partial}{\partial \boldsymbol{\Omega}}(\boldsymbol{F}(\boldsymbol{\Omega}, \boldsymbol{v}_0))|_{\boldsymbol{\Omega}=\boldsymbol{\Omega}_0}(\boldsymbol{\Omega} - \boldsymbol{\Omega}_0) \\ & + \tfrac{\partial}{\partial \boldsymbol{v}}(\boldsymbol{F}(\boldsymbol{\Omega}_0, \boldsymbol{v}))|_{\boldsymbol{v}=\boldsymbol{v}_0}(\boldsymbol{v} - \boldsymbol{v}_0) \\ & + \tfrac{\partial}{\partial \boldsymbol{\omega}}(\boldsymbol{G}(\boldsymbol{\omega}, \dot{\boldsymbol{\omega}}_0))|_{\boldsymbol{\omega}=\boldsymbol{\omega}_0}(\boldsymbol{\omega} - \boldsymbol{\omega}_0) \\ & + \tfrac{\partial}{\partial \dot{\boldsymbol{\omega}}}(\boldsymbol{G}(\boldsymbol{\omega}_0, \dot{\boldsymbol{\omega}}))|_{\dot{\boldsymbol{\omega}}=\dot{\boldsymbol{\omega}}_0}(\dot{\boldsymbol{\omega}} - \dot{\boldsymbol{\omega}}_0) \end{aligned} \tag{2}$$

First it can be recognized that the first two terms give the current angular acceleration and thrust: $\boldsymbol{F}(\boldsymbol{\Omega}_0, \boldsymbol{v}_0) +$

$\boldsymbol{G}(\boldsymbol{\omega}_0, \dot{\boldsymbol{\omega}}_0) = [\dot{\boldsymbol{\Omega}}_0^T \quad T_0]^T$. Furthermore we assume that the moments due to changes in the function $\boldsymbol{F}(\boldsymbol{\Omega}, \boldsymbol{v})$ are small compared to the input moments and can be neglected. Finally, we assume that over the operational domain, the partial derivatives of $\boldsymbol{G}(\boldsymbol{\omega}, \dot{\boldsymbol{\omega}})$ do not change. Therefore, we can approximate them by the static matrices $\boldsymbol{G}_1$ and $\boldsymbol{G}_2$. These control effectiveness matrices are (4×4), because they contain the effectiveness of each of the four rotors on each of the axes roll, pitch, yaw and thrust.

$$\begin{bmatrix} \dot{\boldsymbol{\Omega}} - \dot{\boldsymbol{\Omega}}_0 \\ T - T_0 \end{bmatrix} = \boldsymbol{G}_1(\boldsymbol{\omega} - \boldsymbol{\omega}_0) + T_s \boldsymbol{G}_2(\dot{\boldsymbol{\omega}} - \dot{\boldsymbol{\omega}}_0) \tag{3}$$

Here, the sample time T_s is factored out of $\boldsymbol{G}_2$ to simplify future calculations. The angular acceleration $\dot{\boldsymbol{\Omega}}_0$ can be determined, by deriving it from the gyroscope using finite difference. This signal is often very noisy, because the rotating propellers lead to vibrations in the airframe. From Bacon et al.[22], we adopt the use of a second order filter, given by:

$$H(s) = \frac{\omega_n^2}{s^2 + 2\zeta\omega_n s + \omega_n^2} \tag{4}$$

This filter also introduces a delay. To be able to apply the Taylor expansion, terms with index 0 should be from the same moment in time. This is why all these terms should be filtered with the same filter, such that they are equally delayed. These terms are given the subscript f in Eq. 5.

$$\begin{bmatrix} \dot{\boldsymbol{\Omega}} - \dot{\boldsymbol{\Omega}}_f \\ T - T_f \end{bmatrix} = \boldsymbol{G}_1(\boldsymbol{\omega} - \boldsymbol{\omega}_f) + T_s \boldsymbol{G}_2(\dot{\boldsymbol{\omega}} - \dot{\boldsymbol{\omega}}_f) \tag{5}$$

By approximating $\dot{\boldsymbol{\omega}}$ and $\dot{\boldsymbol{\omega}}_f$ with finite difference, using the lag operator L as $\dot{\boldsymbol{\omega}} = (\boldsymbol{\omega}(k) - \boldsymbol{\omega}(k-1))/T_s = (\boldsymbol{\omega} - L\boldsymbol{\omega})/T_s$ and rearranging the terms, we arrive at:

$$\begin{bmatrix} \dot{\boldsymbol{\Omega}} - \dot{\boldsymbol{\Omega}}_f \\ T - T_f \end{bmatrix} = (\boldsymbol{G}_1 + \boldsymbol{G}_2)(\boldsymbol{\omega} - \boldsymbol{\omega}_f) - \boldsymbol{G}_2 L(\boldsymbol{\omega} - \boldsymbol{\omega}_f) \tag{6}$$

This equation can now be inverted, to yield Eq. 7.

$$\boldsymbol{\omega}_c = \boldsymbol{\omega}_f + (\boldsymbol{G}_1 + \boldsymbol{G}_2)^{-1} \cdot \left(\begin{bmatrix} \boldsymbol{\nu}_{\dot{\boldsymbol{\Omega}}} - \dot{\boldsymbol{\Omega}}_f \\ \widetilde{T} \end{bmatrix} + \boldsymbol{G}_2 L(\boldsymbol{\omega}_c - \boldsymbol{\omega}_f) \right) \tag{7}$$

Here, $\boldsymbol{\nu}_{\dot{\boldsymbol{\Omega}}}$ is the virtual control, which is the desired angular acceleration that has now become an input. In the next section we will show that the thrust increment $T - T_f$ is calculated in the outer loop, and is therefore denoted by $\widetilde{T}$. The subscript c is added to $\boldsymbol{\omega}$ to indicate that this is the command sent to the motors.

The control diagram is shown in Figure 3. The input to this diagram is the angular acceleration virtual control and the output is the angular acceleration of the vehicle. The angular acceleration error, and the thrust increment go into the inversion of the control effectiveness. The increment in motor command is added to the feedback from the motors, which is filtered with the same filter as the angular acceleration. The actuator dynamics are denoted by $A(z)$.

A. Attitude Control

The control law of Eq. 7 describes how to track angular accelerations. A PD controller can be used to provide the angular acceleration that will steer the vehicle towards a desired attitude, as is shown in Figure 4.

In this figure we assume small angles, in order to allow simple integration of the rates to obtain the attitude. In reality, we use a quaternion attitude representation, with the appropriate feedback, as described by Fresk and Nikolakopoulos [23]. That means that the proportional gain for the quaternion representation has to be twice as large as K_η from Figure 4, since the quaternion derivative is defined as:

$$\dot{\boldsymbol{q}} = \frac{1}{2}\boldsymbol{q} \otimes \begin{bmatrix} 0 \\ \boldsymbol{\Omega} \end{bmatrix} \tag{8}$$

where $\otimes$ denotes the Hamilton product. In previous research [14] we have shown that if the assumptions, mentioned in the derivation of the controller, hold true, the transfer function from $\boldsymbol{\nu}_{\dot{\boldsymbol{\Omega}}}$ to $\dot{\boldsymbol{\Omega}}$ is simply the actuator dynamics $\boldsymbol{A}(z)$. When the actuator dynamics can be modeled, for instance by first order dynamics, the P and D gains can be determined based on the desired poles and zeros of the system. For the Bebop, the actuator dynamics are modeled with first order dynamics as shown in Eq. 9, with $\alpha = 0.1$.

$$A(z) = \frac{\alpha}{z - (1 - \alpha)} \tag{9}$$

Then the transfer function of the closed loop system from Figure 4 is as follows:

$$TF_{\eta_{\text{ref}} \to \eta} = \frac{K_\Omega K_\eta \alpha T_s^2}{z^3 - (3-\alpha)z^2 + (3 - 2\alpha + K_\Omega \alpha T_s)z + (-1 + \alpha - K_\Omega \alpha T_s + K_\Omega K_\eta \alpha T_s)} \tag{10}$$

With $K_\Omega = 28$ and $K_\eta = 10.7$, there is one pole at 0.964 and two complex poles at 0.968±0.0463. All poles are within the unit circle and the response is fast with little overshoot.

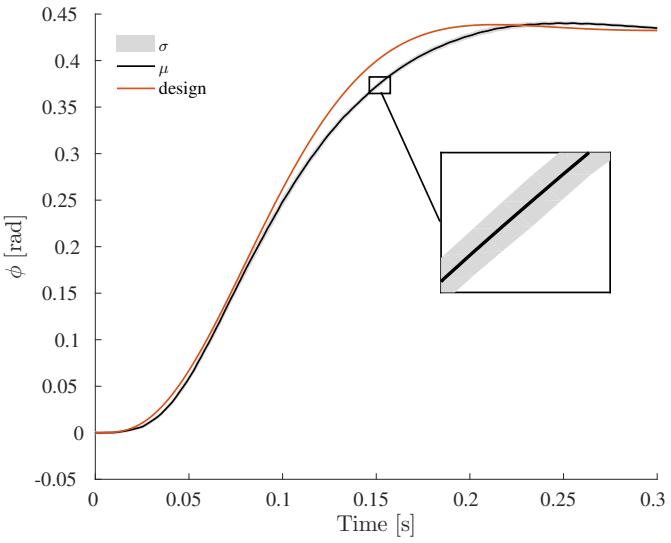

Fig. 5. Comparison of the designed response and the actual response of the attitude of the quadrotor. The black line is the average, and the gray area one standard deviation of 25 repetitions.

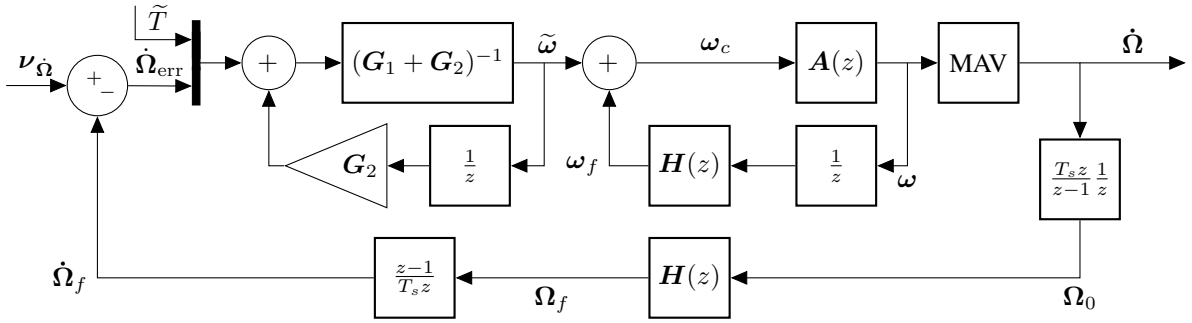

Fig. 3. The inner INDI control structure.

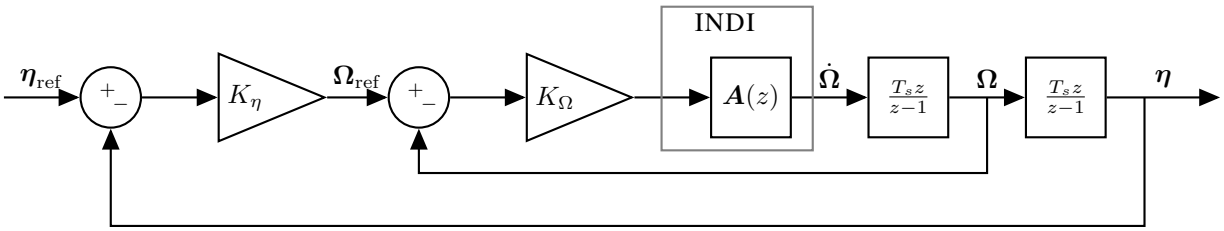

Fig. 4. The design of the attitude controller for small angles, based on the closed loop response of the INDI controller.

An interesting question is how close the theoretically designed response of the attitude matches the actual attitude response of the quadrotor. To test this, we subject both the above transfer function and the real quadrotor to a step input. For the real quadrotor, the step input is repeated 25 times, and the mean and standard deviation are shown in Figure 5. The response of the above transfer function is shown in the same figure in red. The difference between the designed response and the actual response is rather small: the error as a percentage of the step magnitude is maximum 6.4 % at 0.14 s. This means that this is a valid way of designing the P and D gains, based solely on the first order actuator dynamics model.

III. Incremental Nonlinear Dynamic Inversion Applied to Linear Accelerations

Now that we have a controller that controls the attitude of the quadrotor, we can derive an incremental controller for the linear acceleration of the vehicle. Two reference frames will be used throughout this derivation; the body frame, as depicted in Figure 2, and the North East Down (NED) frame. Vectors in the body frame have a subscript B and vectors in the NED frame have subscript N. The subscripts will only be used to avoid confusion, the position $\boldsymbol{\xi}$ and velocity $\dot{\boldsymbol{\xi}}$ of the quadrotor will always be in the NED frame.

The position dynamics are given by Newton's second law of motion:

$$\ddot{\boldsymbol{\xi}} = \boldsymbol{g} + \frac{1}{m}\boldsymbol{F}(\dot{\boldsymbol{\xi}}, \boldsymbol{w}) + \frac{1}{m}\boldsymbol{T}_N(\boldsymbol{\eta}, T) \tag{11}$$

Where $\ddot{\boldsymbol{\xi}}$ is the acceleration of the MAV, $\boldsymbol{g}$ is the gravity vector and m is the mass. $\boldsymbol{F}$ is the aerodynamic force working on the airframe as a function of the velocity $\dot{\boldsymbol{\xi}}$ of the MAV and the wind vector $\boldsymbol{w}$. $\boldsymbol{T}_N$ is the thrust vector in the NED frame as a function of the attitude $\boldsymbol{\eta} = [\phi, \theta, \psi]^T$ and the total thrust produced by the four rotors T.

The thrust vector in the NED frame can be obtained by taking the thrust vector in the body frame, given by $\boldsymbol{T}_B = [0, 0, T]^T$, and rotating it using the rotation matrix $\boldsymbol{M}_{NB}(\boldsymbol{\eta})$. Since the thrust vector in the body frame only has a Z component, only the last column of the rotation matrix is relevant. The thrust vector in the NED frame is therefore given by:

$$\boldsymbol{T}_N(\boldsymbol{\eta}, T) = \boldsymbol{M}_{NB}(\boldsymbol{\eta})\boldsymbol{T}_B = \begin{bmatrix} (\mathrm{s}\phi\mathrm{s}\psi + \mathrm{c}\phi\mathrm{c}\psi\mathrm{s}\theta)T \\ (\mathrm{c}\phi\mathrm{s}\psi\mathrm{s}\theta - \mathrm{c}\psi\mathrm{s}\phi)T \\ (\mathrm{c}\phi\mathrm{c}\theta)T \end{bmatrix} \tag{12}$$

where the sine and cosine functions are abbreviated by the letters s and c respectively. Now we can apply a first order Taylor expansion to Eq. 11, resulting in Eq. 13:

$$\begin{aligned} \ddot{\boldsymbol{\xi}} = \quad & \boldsymbol{g} + \tfrac{1}{m}\boldsymbol{F}(\dot{\boldsymbol{\xi}}_0, \boldsymbol{w}_0) + \tfrac{1}{m}\boldsymbol{T}_N(\boldsymbol{\eta}_0, T_0) \\ & + \tfrac{\partial}{\partial \dot{\boldsymbol{\xi}}}\tfrac{1}{m}\boldsymbol{F}(\dot{\boldsymbol{\xi}}, \boldsymbol{w}_0)|_{\dot{\boldsymbol{\xi}}=\dot{\boldsymbol{\xi}}_0}(\dot{\boldsymbol{\xi}} - \dot{\boldsymbol{\xi}}_0) \\ & + \tfrac{\partial}{\partial \boldsymbol{w}}\tfrac{1}{m}\boldsymbol{F}(\dot{\boldsymbol{\xi}}_0, \boldsymbol{w})|_{\boldsymbol{w}=\boldsymbol{w}_0}(\boldsymbol{w} - \boldsymbol{w}_0) \\ & + \tfrac{\partial}{\partial \boldsymbol{\phi}}\tfrac{1}{m}\boldsymbol{T}_N(\boldsymbol{\eta}, T_0)|_{\phi=\phi_0}(\phi - \phi_0) \\ & + \tfrac{\partial}{\partial \boldsymbol{\theta}}\tfrac{1}{m}\boldsymbol{T}_N(\boldsymbol{\eta}, T_0)|_{\theta=\theta_0}(\theta - \theta_0) \\ & + \tfrac{\partial}{\partial T}\tfrac{1}{m}\boldsymbol{T}_N(\boldsymbol{\eta}_0, T)|_{T=T_0}(T - T_0) \end{aligned} \tag{13}$$

The first term can be simplified to the acceleration at the previous timestep: $\boldsymbol{g} + \frac{1}{m}\boldsymbol{F}(\dot{\boldsymbol{\xi}}_0) + \frac{1}{m}\boldsymbol{T}_N(\boldsymbol{\eta}_0, T_0) = \ddot{\boldsymbol{\xi}}_0$. This acceleration can be obtained by rotating the specific force measured by the accelerometer in the body axes to the NED frame and adding the gravity vector. For the next two terms, the partial derivative of $\boldsymbol{F}$ with respect to $\dot{\boldsymbol{\xi}}$ and $\boldsymbol{w}$, we do not have a good estimate. For simplicity of the approach, we choose not to employ a model of the aerodynamic drag of the airframe. Moreover, it is very difficult, if not impossible, to

predict how the wind is going to change. Therefore, the best guess for these terms is zero. Note that this does not mean that all aerodynamic forces are neglected. These forces will be measured with $\ddot{\boldsymbol{\xi}}_0$. Combining this with Eq. 12 and 13 we end up with:

$$\ddot{\boldsymbol{\xi}} = \ddot{\boldsymbol{\xi}}_0 + \frac{1}{m} G(\boldsymbol{\eta}_0, T_0)(\boldsymbol{u} - \boldsymbol{u}_0) \tag{14}$$

where $\boldsymbol{u} = \begin{bmatrix} \phi & \theta & T \end{bmatrix}^T$ and

$$\boldsymbol{G}(\boldsymbol{\eta}, T) = \begin{bmatrix} (\mathrm{c}\phi\mathrm{s}\psi - \mathrm{s}\phi\mathrm{c}\psi\mathrm{s}\theta)T & (\mathrm{c}\phi\mathrm{c}\psi\mathrm{c}\theta)T & \mathrm{s}\phi\mathrm{s}\psi + \mathrm{c}\phi\mathrm{c}\psi\mathrm{s}\theta \\ (-\mathrm{s}\phi\mathrm{s}\psi\mathrm{s}\theta - \mathrm{c}\psi\mathrm{c}\phi)T & (\mathrm{c}\phi\mathrm{s}\psi\mathrm{c}\theta)T & \mathrm{c}\phi\mathrm{s}\psi\mathrm{s}\theta - \mathrm{c}\psi\mathrm{s}\phi \\ -\mathrm{c}\theta\mathrm{s}\phi T & -\mathrm{s}\theta\mathrm{c}\phi T & \mathrm{c}\phi\mathrm{c}\theta \end{bmatrix} \tag{15}$$

The measured accelerations, necessary to obtain $\ddot{\boldsymbol{\xi}}_0$, are typically noisy due to vibrations in the airframe introduced by the spinning propellers. Therefore, the accelerations need to be filtered. Like in the previous section, the delay of the filter needs to be accounted for. This is why also here, all terms with subscript 0 will be filtered with the same filter, and be given a subscript f. Then, if we invert Eq. 14, we obtain the INDI control law for linear accelerations:

$$\boldsymbol{u}_c = \boldsymbol{u}_f + mG^{-1}(\boldsymbol{\eta}_0, T_0)(\boldsymbol{\nu}_{\ddot{\xi}} - \ddot{\boldsymbol{\xi}}_f) \tag{16}$$

We have replaced $\ddot{\boldsymbol{\xi}}$ with the virtual control $\boldsymbol{\nu}_{\ddot{\xi}}$ to indicate that this is now an input to the equation (the desired acceleration), and we added the subscript c to $\boldsymbol{u}$ to indicate that this is the command that will be sent to the inner loop controller. We also define the control increment to be $\widetilde{\boldsymbol{u}} = \boldsymbol{u}_c - \boldsymbol{u}_f$, so clearly Eq. 16 is an incremental control law.

Suppose we filter the inner loop with filter f_1, and the outer loop with filter f_2. The thrust increment required by the inner loop is then $T - T_{f_1}$. The thrust increment calculated by the outer loop is $T - T_{f_2}$. We can only pass on the thrust increment from the outer to the inner loop if these filters are equal. That is why for both loops, we use the filter described by Eq. 4, with the same parameters.

IV. Implementation

The implementation of the control law given by Eq. 16 is shown in Figure 6. The input of this diagram is the virtual control, and the output is the acceleration in NED frame. The acceleration in NED frame can be obtained from the accelerometer measurements with a simple rotation matrix and the addition of the gravity vector. Increments in roll, pitch and thrust are obtained from the error in acceleration multiplied with the inverse of the control effectiveness matrix. The roll and pitch increments are added to the filtered measurement of roll and pitch. Note how the increment in thrust command $\widetilde{T}$ goes directly into the inner loop.

A. Position Control

In the previous sections, we have shown how the linear acceleration can be controlled using an INDI controller. To control the position of the MAV, an acceleration reference needs to be passed to the outer INDI controller that will steer the MAV towards its target position. This can be done by a Proportional Derivative (PD) controller, as is shown in Figure 7. The gains of this PD controller were manually tuned.

They depend mainly on two things: the update rate of the position estimate and the speed of the inner loop controller, which is only dependent on the actuator dynamics. This is the case because all other components are inverted in the inversion step of the inner and outer loop. Therefore, if these parameters are known in advance, one can come up with an estimate of the PD gains, for instance based on a pole/zero analysis.

B. Adaptive Control Effectiveness

In our previous work we used a Least Mean Squares algorithm to adapt the control effectiveness matrix of the rotors online. Now, with respect to our previous work, we have added a row to the control effectiveness matrix that predicts a change in thrust based on the actuator inputs. This row of the control effectiveness matrix can also be adapted online, together with the rest of the matrix. The LMS algorithm then becomes:

$$\begin{aligned} &\boldsymbol{G}(k) = \boldsymbol{G}(k-1) \\ &-\boldsymbol{\mu}_2 \left(\boldsymbol{G}(k-1) \begin{bmatrix} \Delta\boldsymbol{\omega}_f \\ \Delta\dot{\boldsymbol{\omega}}_f \end{bmatrix} - \begin{bmatrix} \Delta\dot{\boldsymbol{\Omega}}_f \\ \Delta T \end{bmatrix} \right) \begin{bmatrix} \Delta\boldsymbol{\omega}_f \\ \Delta\dot{\boldsymbol{\omega}}_f \end{bmatrix}^T \boldsymbol{\mu}_1 \end{aligned} \tag{17}$$

Where:

$$\boldsymbol{G}(k) = \begin{bmatrix} \boldsymbol{G}_1(k) & \boldsymbol{G}_2(k) \end{bmatrix} \tag{18}$$

This means that the effectiveness of the motors with respect to the thrust can also be adapted online. This can be important if the weight of the vehicle changes during flight, for instance when dropping a payload. Given a flight with enough excitation of the control input and limited disturbances, the control effectiveness converges to the control effectiveness calculated offline.

C. Estimation of the Thrust

Throughout the derivation of the outer loop INDI controller, we made use of the thrust T, for instance in the matrix $G(\boldsymbol{\eta}, T)$. One possibility would be to measure the specific force in the body Z axis with the accelerometer, and use this as an estimate for the specific thrust ($\frac{T}{m}$). This approach works well while hovering, but can lead to errors when there are other (aerodynamic) forces in the body Z axis. These forces occur for instance at high speed steady flight, when the drone has a high bank angle.

Therefore, we used static thrust measurements to model the thrust/rotational rate curve of the propellers. The quadrotor was mounted upside down on a scale to obtain a measurement of the produced thrust. The rotational rate of the propellers was obtained from the internal rpm measurement. The results are shown in Figure 8. A quadratic function showed a good fit with the data. This function is used for the thrust estimate in the calculations of the controller.

Of course, the actual thrust of the propellers may be slightly different in a real flight, due to a different inflow. Furthermore, since the propellers have a quadratic thrust curve, their control effectiveness changes depending on their current rotational rate. In this paper, we assume that the control effectiveness

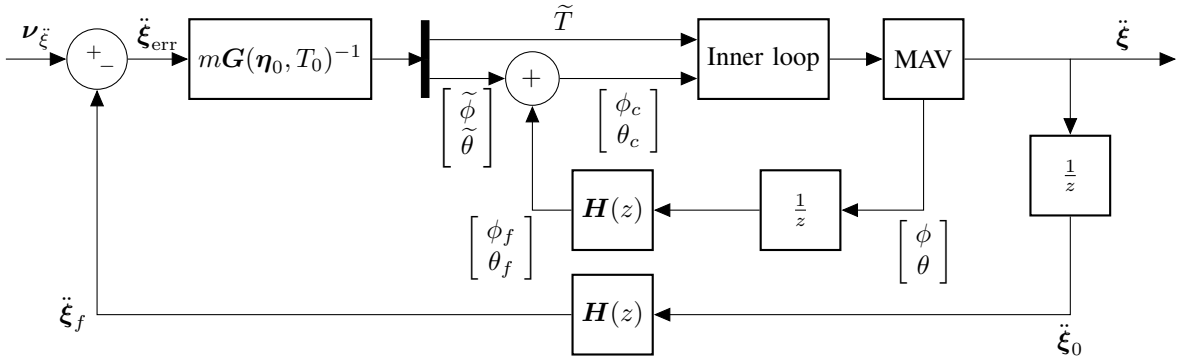

Fig. 6. The outer INDI control structure.

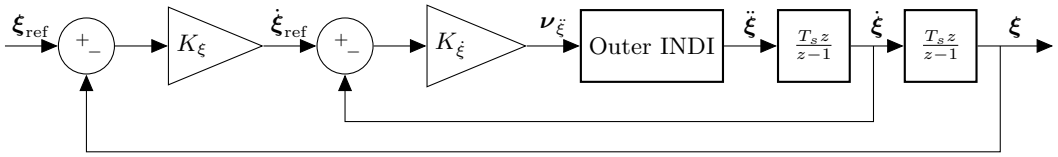

Fig. 7. The PD controller for the position.

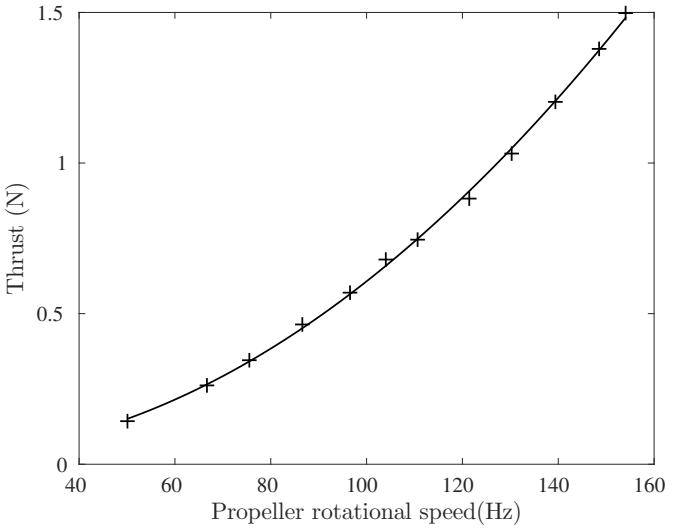

Fig. 8. Thrust measurements for different rotor speeds along with a second order approximation.

of the rotors with respect to the specific force can be approximated by a static one. This removes the need to recalculate $(\boldsymbol{G}_1 + \boldsymbol{G}_2)^{-1}$ after every time step, enhancing the speed of the algorithm.

Errors introduced by these simplifications are expected to have low impact, because of the incremental nature of the controller. If an increment in thrust does not lead to the desired acceleration, another increment is applied. This way, small errors in the control effectiveness are handled naturally.

D. Linearization

In the previous section, we used a first order Taylor expansion to derive the INDI control law. However, from Equation 12 it can be seen that the force is actually very nonlinear in terms of roll and pitch. In Equation 15 it can be seen that some of the derivatives can even change sign, for instance $\frac{\partial \ddot{z}}{\partial \phi}$ for different values of ϕ.

What this means in practice is that if the increments in the input are large, because suddenly a large lateral acceleration is required, they will result in a different acceleration than intended. This will be measured by the accelerometer, and subsequent increments in the inputs will eventually lead to the right acceleration. But it might be more effective to implement a nonlinear method of finding increments in the input that give exactly the desired increment in the acceleration.

Since we have the nonlinear function of our inputs available, it is possible to do a nonlinear inversion. At the same time, we would like to keep the incremental structure, because we don't have an accurate estimate of the aerodynamic forces $\boldsymbol{F}$. If we refer to Eq. 11, we can subtract the same formula a short time instant earlier:

$$\begin{aligned}\ddot{\boldsymbol{\xi}} - \ddot{\boldsymbol{\xi}}_0 = \; & \boldsymbol{g} - \boldsymbol{g}_0 + \tfrac{1}{m}\boldsymbol{F}(\dot{\boldsymbol{\xi}}, \boldsymbol{w}) - \tfrac{1}{m}\boldsymbol{F}(\dot{\boldsymbol{\xi}}_0, \boldsymbol{w}_0) \\ & + \tfrac{1}{m}\boldsymbol{T}_N(\boldsymbol{\eta}, T) - \tfrac{1}{m}\boldsymbol{T}_N(\boldsymbol{\eta}_0, T_0)\end{aligned} \tag{19}$$

We assume changes in gravity and the aerodynamic forces are small during this small time instant:

$$\ddot{\boldsymbol{\xi}} - \ddot{\boldsymbol{\xi}}_0 = \frac{1}{m}\boldsymbol{T}_N(\boldsymbol{\eta}, T) - \frac{1}{m}\boldsymbol{T}_N(\boldsymbol{\eta}_0, T_0) \tag{20}$$

If we desire a different acceleration, we now know what the increment in the thrust vector should be. We can calculate what the current thrust vector is based on the attitude and rotational rate of the rotors. This gives an expression for the new thrust vector:

$$\boldsymbol{T}_N(\boldsymbol{\eta}, T) = m(\ddot{\boldsymbol{\xi}} - \ddot{\boldsymbol{\xi}}_0) + \boldsymbol{T}_N(\boldsymbol{\eta}_0, T_0) \tag{21}$$

How the thrust vector depends on the thrust and attitude is described by Eq. 12. We can do a nonlinear inversion of this

equation to obtain expressions for the thrust, roll and pitch commands:

$$T = ||\boldsymbol{T}_N|| \tag{22}$$

$$\phi_c = \arcsin\left(\frac{\sin(\psi)T_{N_x} - \cos(\psi)T_{N_y}}{T}\right) \tag{23}$$

$$\theta_c = \arcsin\left(\frac{\cos(\psi)T_{N_x} + \sin(\psi)T_{N_y}}{T\cos\phi_c}\right) \tag{24}$$

This allows us to find a new attitude and thrust that will satisfy a desired acceleration, without linearizing the input function. At the same time, we have retained the incremental structure, as we calculate the new thrust vector based on the previous one. For the nonlinear case, the same argument holds regarding the filtering as for the linearized case: if we filter the acceleration, we should also filter the other signals with subscript 0. This is shown below:

$$\boldsymbol{T}_N(\boldsymbol{\eta}, T) = m(\ddot{\boldsymbol{\xi}} - \ddot{\boldsymbol{\xi}}_f) + \boldsymbol{T}_N(\boldsymbol{\eta}_f, T_f) \tag{25}$$

E. Filtering

Both the measured accelerations as well as the rates are filtered to remove noise. In the derivation of the INDI controller, we showed that these signals should be filtered with the same filter. This way, the delay in both loops is synchronized and the thrust increment can go from the outer loop to the inner loop.

Previously, we have shown that the filter choice has an effect on the disturbance rejection [14]. For the attitude loop, the response to a disturbance is given by $(1 - A(z)H(z)z^{-1})$. By taking a filter with a higher cutoff frequency, and therefore less delay, disturbances will be rejected faster. On the other hand, more noise will end up in the control signals. Since the inner and outer INDI loops are connected and need to use the same filter, this trade-off should be considered for both loops simultaneously. For the experiment, we chose a filter with a $\omega_n = 50$ rad/s and $\zeta = 0.55$.

F. Accelerometer Bias

The outer loop INDI controller is somewhat sensitive to accelerometer biases. Because the accelerometer measurement is fed back to control the acceleration, an offset in the measurement will result in an offset in the actual acceleration as well. This means that the quadrotor will maintain its position not at a position with zero error, but at a position where the position error times the P gain gives a required acceleration equal to minus the acceleration offset.

This problem does not arise in the inner loop, where the angular acceleration is bias free. This is because in calculating the derivative of the rates, the bias disappears from the signal. This is not the case for the outer loop, so we need to estimate the accelerometer bias in order to remove it. As a second measurement we have the velocity and position from GPS or an indoor positioning system. The velocity measurement can be derived to obtain a bias free acceleration measurement. The measurement of the velocity only has a low update rate, so this signal is not really viable for feedback.

However, the acceleration obtained from velocity can be used to determine the accelerometer bias. The accelerometer bias is a signal that is assumed to vary only very slowly. This is why we filter both the accelerometer and the acceleration obtained from the velocity measurement with a second order filter with a natural frequency of 0.25 rad/s. This removes all noise while keeping the important bias information. The signals are both filtered with the same filter such that they have the same delay. After the filtering, the signals are subtracted to find the accelerometer bias. This is only a very simple method of finding the accelerometer bias, it could alternatively be done with a Kalman filter.

V. Windtunnel Experiment

The goal of the experiment is to test how well the INDI controller can handle gust disturbances. The experiment is performed indoors, such that there is a controlled environment in which repeatable experiments can be performed. The source of the wind disturbance is the Open Jet Facility of the TU Delft Aerospace department. It has a 2.85 m by 2.85 m cross section, and is capable of velocities up to 30 m/s. A picture of the drone flying in front of the windtunnel is shown in Figure 1. Because the windtunnel is not capable of rapidly increasing or decreasing its velocity, the quadrotor has to fly in and out of the windtunnel exhaust to simulate a gust. This is done by letting the quadrotor alternate between two waypoints every 14 seconds, one being in the center of the of the windtunnel exhaust, and one being 2 meters west of this point.

The INDI loop basically controls the acceleration of the MAV. From this perspective, it is an addition to a PID controller, where with INDI the integral gain is zero. This is why we will compare the performance of INDI with a regular PID controller. The PID controller is manually tuned to give the fastest response possible without oscillation. Both the INDI as well as the PID outer loop controllers make use of the inner loop INDI controller for attitude control. For the PID controller, the P, I and D gains work directly on the position and velocity to produce a reference roll, pitch and thrust. In tuning these gains, there is a trade-off to be made. By increasing the integral gain, faster offset compensation can be obtained. This way the quadrotor can adjust to the disturbance of the windtunnel faster. However, with a high integral gain, the quadrotor will also have more overshoot in reference tracking tasks such as sudden position changes. This trade-off is non-existent for the INDI controller.

We can do a crude comparison between the K_ξ and $K_{\dot{\xi}}$ gains of the INDI controller and the P and D gains of the PID controller. Around hover, the virtual control is related to the change in commanded attitude angle through a division by gravity, assuming small angles. K_ξ and $K_{\dot{\xi}}$ then become 0.70 (m/s)/m and 0.15 rad/(m/s) respectively. For the PID controller, the corresponding P and D gains are 0.65 (m/s)/m and 0.20 rad/(m/s) respectively. Though these gains are not exactly the same, the goal of this crude comparison is to show that both controllers have roughly the same gains. Since we

will consider disturbance rejection properties, the integral gain will play the biggest role.

The MAV used for the experiments is the Bebop quadrotor from Parrot. Instead of the stock firmware, it is running the Paparazzi open source autopilot system. An infrared motion tracking system called 'Optitrack' was used to obtain position information. This system can measure the drone's position with millimeter accuracy at a frequency up to 120 Hz. But because we want the experiment to be realistic for outside scenarios and since most Global Positioning System (GPS) modules can only provide position updates at four Hz, the data was only sent to the drone at a frequency of four Hz. The control algorithm, as well as the onboard accelerometer and gyroscope, were running at 512 Hz. In an outdoor scenario, millimeter accuracy might not be achievable with off the shelve GPS modules. But even though the position might be off in such a case, gusts will still be rejected the same way as in this indoor experiment, as the INDI controller is based on the accelerometer.

A. Results

First, consider Figure 9. It shows the acceleration in the north axis, which is the axis in which the windtunnel is blowing. The acceleration is filtered with a second order filter with $\omega_n = 20$ rad/s and $\zeta = 0.7$. At 113.6 seconds, the quadrotor is commanded to fly into the wind. The moment the quadrotor flies into the wind stream is clearly visible in the figure due to the large acceleration spike, deviating from the reference acceleration. Due to this acceleration error, the INDI controller will increment the control inputs in order to make the acceleration track the reference again. About half a second after the start of the disturbance, the acceleration coincides with the reference acceleration, effectively having counteracted the disturbance. At that point, the quadcopter has built up a speed and position error in the north axis. The quadrotor needs a positive acceleration after the disturbance to bring these errors back to zero.

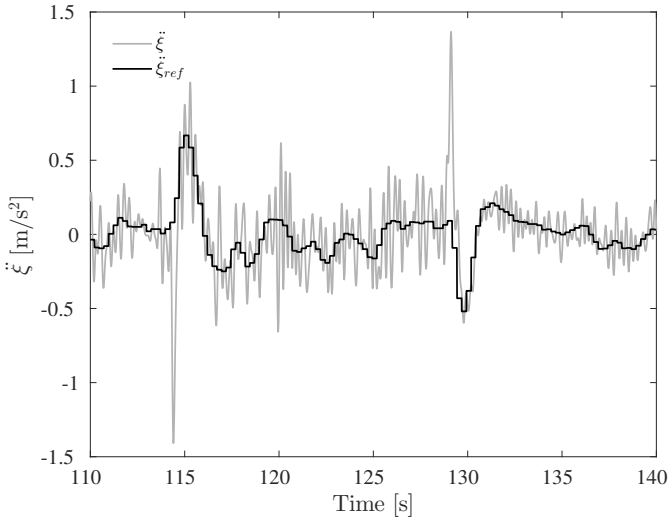

Fig. 9. Acceleration in the north direction for the INDI controller.

The same thing happens at 127.5 seconds, when the quadrotor is commanded to fly out of the wind again. Now the sudden absence of wind results in a disturbance in the opposite direction. What also can be observed from this figure is that the accelerometer measures a more high frequency signal when flying in the wind. This could be due to the airflow containing some turbulence.

Figure 10 shows the position along the X_N axis, for both the INDI and PID controllers. The Figure shows the average of seven times the same maneuver, along with one standard deviation. For INDI, we can observe that a position error of 0.2 m occurs upon entering (113.6 seconds) or leaving (127.5 seconds) the windtunnel. This position error is counteracted within three seconds after it occurred.

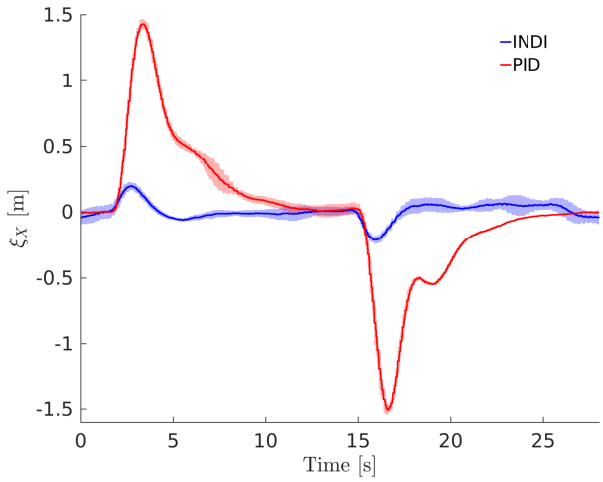

Fig. 10. Position in the North direction for the INDI and PID experiment. The line is the average of seven repetitions, and the colored areas indicate one standard deviation.

Compare this with the position for the PID controller in the same figure. The maximum error is 1.5 m, and it takes longer for the position error to be counteracted as compared to the INDI controller. One thing to note is that, when the vehicle is flying in the windtunnel (20-28 seconds) and there are no changing disturbances, there is very little variance between flights. This difference may be attributed to the fact that the INDI controller is using the accelerometer for feedback. Though the accelerometer measurement is filtered, it is still a bit noisy. A filter with more high frequency attenuation could have been used, but this would make the disturbance rejection of the controller slightly slower, because such a filter has more delay.

A top view of the experiment is shown in figure 11. From this figure the difference in performance becomes apparent. The Figure shows the entire flight, from takeoff until landing. For the PID controller, you can see how it is blown in the negative X_N direction upon takeoff, entering the windtunnel, and how it overshoots in a straight line upon landing, leaving the windtunnel flow. The INDI controller is able to cope much better with the sudden wind changes during taking off and landing.

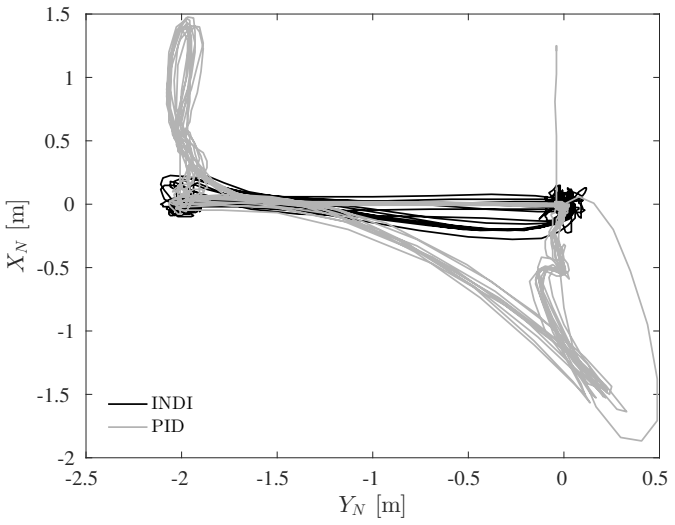

Fig. 11. Top view of the experiment for the PID and INDI controllers at 10 m/s.

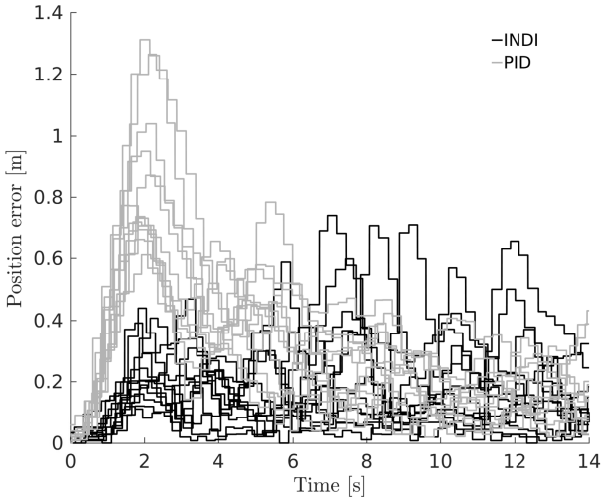

Fig. 12. The horizontal position error during the outdoor takeoff experiment.

VI. Outdoor Takeoff with Wind

The experiment in the windtunnel is great from a scientific point of view, as it allows us to compare different controllers subject to exactly the same disturbance. On the other hand, since we used an Optitrack system for position estimation, it might not be clear if the controller can provide the same performance in an outdoor scenario. That is why we performed a second experiment; outdoors and with a standard off-the-shelve GPS receiver.

One of the situations in which an MAV needs to cope with a sudden wind disturbance, is during takeoff on a windy day. When on the ground, the ground is compensating the drag from the wind. But when the drone takes off, the wind force will accelerate the drone. Therefore, a control action is needed to counteract the wind and maintain position.

Since the acceleration is measured with the accelerometer, it is expected that the INDI controller will compensate for the wind force very fast. A PID controller that does not use this information, on the other hand, is expected to drift a bit, until it has gained some error in position and velocity that causes it to steer back. The integrator part will remove the steady state error over time.

Like before, we are using the first version of the Bebop quadrotor for this experiment. As opposed to the second version of the Bebop, the first version that is used for this experiment has a low quality GPS. With the built-in GPS, the disturbance rejection performance is hard to evaluate, as the position estimate will move around quite a bit, regardless if the drone is moving or not. This is why the quadrotor is equipped with an external Ublox Neo M8N through a USB connection. This GPS module is commercially available, and the second version of the Bebop even ships with this module built in.

Like the windtunnel experiment, we will compare the case with outer loop INDI and without. The PID controller has the same gains as in the windtunnel experiment, just like the P and D gains that produce the acceleration reference for the INDI controller are the same.

A. Results

On the day of the outdoor takeoff experiment an average wind speed of 5.1 m/s was reported by the Dutch Meteorological Institute (KNMI). Over the course of one and a half hour, first twelve flights were performed with the PID controller, and then thirteen with the INDI controller. The flights were performed one after the other, without breaks. It is assumed that on average, the wind during the INDI flights was the same as during the PID flights, even though a fluctuation of the wind speed between flights was observed.

One of the flights with the INDI controller was rejected, as from the data it became clear that the state estimation filter had not converged prior to takeoff. The state estimation error leads to a bias in the NED acceleration, which in turn leads to a position offset, as discussed above.

The position error can be seen in Figure 12. The average position error is shown in Figure 13.

The position reference was reset to the current position just before each flight, so all flights start with a position error close to zero. As expected, during the takeoff INDI performs much better than the PID controller. It can be seen from Figure 13 that the INDI controller produces on average a maximum position error of 0.24 m as compared to 0.85 m for the PID controller.

Though Figure 13 shows that the average error after some time is the same for both controllers, it appears from Figure 12 that there are some runs for the INDI controller with relatively large errors. These errors are especially large if they are compared to the position error that is the result of the takeoff in the wind, which was expected to be the main disturbance. Closer inspection of some of these datasets show that when these errors occur, the acceleration measured by the accelerometer does not correspond with the position and velocity measured by the GPS. This may indicate that these errors are caused by by GPS errors, perhaps upon changing between satellites. This could perhaps be solved with a better state estimation algorithm, but that is beyond the scope of this

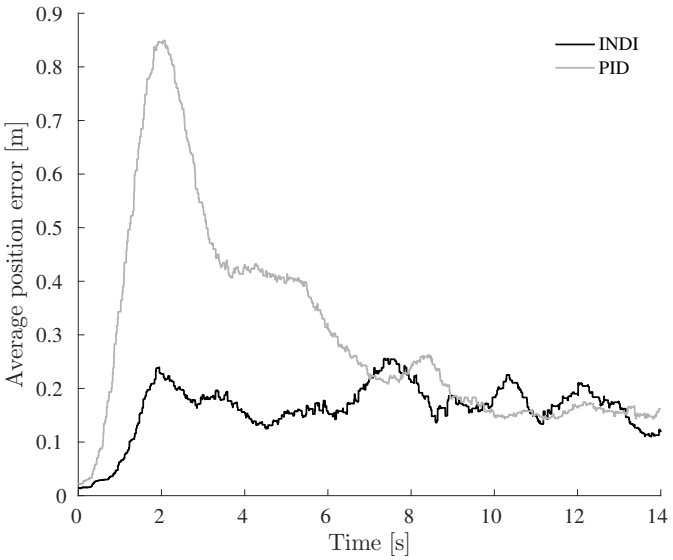

Fig. 13. The average horizontal position error during the outdoor takeoff experiment.

research.

VII. Nonlinear Increment

As described in the section Implementation, the increment in thrust vector $\boldsymbol{T}_N(\boldsymbol{\eta}, T)$ can also be computed without linearizing. The linearization will give a small error if the virtual control $\boldsymbol{\nu}_{\ddot{\boldsymbol{\xi}}}$ is small. But for large values of $\boldsymbol{\nu}_{\ddot{\boldsymbol{\xi}}}$, the error will be more significant.

It might be the case that, while such an incorrect increment in thrust vector is being executed and the quadrotor is rotating, a difference with the expected acceleration is already measured, and subsequent increments correct the thrust increment such that it will give the desired acceleration. It will depend for a large part on the cutoff frequency of the measurement filter if this will be fast enough. If the cutoff frequency of the filter is low, the delay may make the rejection of this disturbance too slow.

To assess whether the linearization is accurate enough for large acceleration changes, an experiment is devised. In this experiment, from a hover initial condition, the quadrotor is commanded an acceleration of (0,4,0) m/s^2 for half a second, and then (0,-4,0) m/s^2 for another half second. This way, it will go from accelerating in one direction, to accelerating in the other direction, resulting in a large acceleration change. The maneuver takes place in the Y-axis, but we expect considerable response differences in the Z-axis.

This flight plan will be used for the Bebop quadrotor controlled with linearized INDI and nonlinear INDI. For the linearized version is expected that, because of the derivative of the vertical component of $\boldsymbol{T}_N(\boldsymbol{\eta}, T)$ with respect to thrust, the quadrotor will suddenly give very little thrust when the large change in acceleration is commanded. Due to this sudden decrease in thrust, the quadrotor is expected to slightly descend, before the vertical acceleration is measured and the thrust is increased again. For the nonlinear version it is expected that the thrust command will remain roughly the same, and little change in altitude is expected.

The experiment will be performed in the indoor flight arena facility at the faculty of Aerospace Engineering in Delft. The quadrotor is hovering based on the position feedback it receives from the tracking system. It does not use this position information during the maneuvers, because the acceleration reference during these maneuvers is predefined. The control effectiveness matrices $\boldsymbol{G}_1$ and $\boldsymbol{G}_2$ were determined prior to the experiment using the adaptive algorithm. The experiment is done with 25 repetitions for both conditions.

A. Results

Figure 14 shows the acceleration in the Z axis of the NED frame for the linearized case. In the first two deciseconds, when the quadrotor is commanded to accelerate in the Y direction, the quadrotor has a slight upward acceleration, even though the thrust increment command at time zero is close to zero. This can be explained with the fact that the inner loop control effectiveness inversion is linear, and will add as much RPM on one side of the quadrotor as on the other side to make it bank. Actually, the relation between RPM and thrust is nonlinear (see Figure 8), and if all propellers are spinning equally fast, a bank command will therefore result in a slight thrust increase.

More profound is the downward acceleration that happens after half a second, when the quadrotor has to accelerate in the -Y direction. Because the quadrotor is banking to facilitate the acceleration in the +Y direction, the derivative of the vertical acceleration with respect to the bank angle is negative (upward acceleration) for a reduction in bank angle. Therefore, even though eventually around the same thrust is required, initially the thrust is reduced significantly, resulting in a downward acceleration.

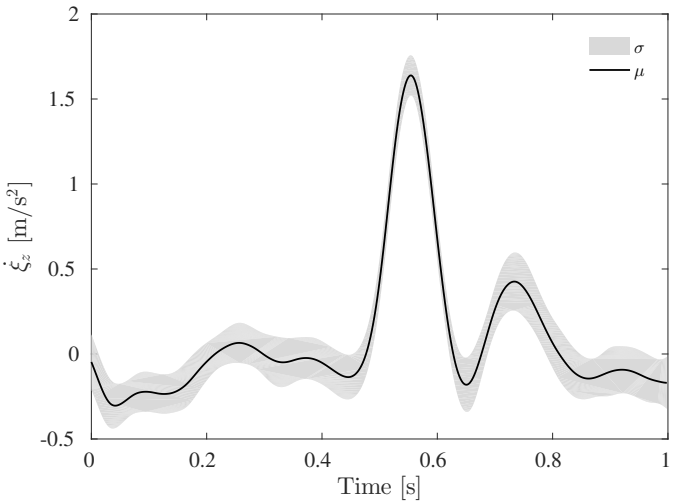

Fig. 14. Acceleration in the NED Z axis with INDI increments calculated through linearization. From 25 experiments we show the mean μ and one standard deviation σ.

Compare this with Figure 15, which shows the nonlinear case. Here a larger acceleration is visible in the first two

deciseconds. This is caused by the fact that the actuator dynamics are faster than the rotational dynamics. The nonlinear increment is calculated for the tilted thrust vector, therefore a positive thrust increment is commanded by the outer loop INDI controller. However, the rotational dynamics are slower than the thrust dynamics. Therefore, the thrust is increased already before the final attitude is attained. This causes the vehicle to accelerate upwards initially.

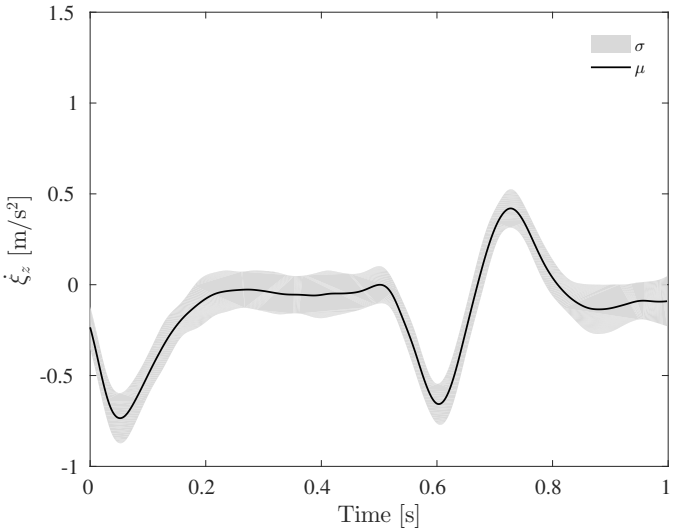

Fig. 15. Acceleration in the NED Z axis with INDI increments calculated through nonlinear calculation. From 25 experiments we show the mean μ and one standard deviation σ.

After half a second, when the large acceleration change is commanded, the response is quite different from the linear case. Instead of acceleration downward, the vehicle accelerates upward. This can be explained by recognizing that the quadrotor will need more or less the same bank angle to accelerate with the same amount in the other direction. This means that the same thrust is needed. However, while the vehicle is rotating, it passes the point of zero bank angle, for which it actually needs less thrust to avoid a vertical acceleration. This can explain that the vehicle accelerates upward, reduces thrust, and then overshoots to downward acceleration when it reaches the bank angle at which increased thrust is needed.

Comparing, the nonlinear implementation results in a vertical acceleration that averages better to the intended zero m/s^2. However, there is still quite some unintended vertical acceleration present. One thing that could improve this is by taking the nonlinear thrust curve into account for the inner loop as well. These acceleration changes were the largest possible without introducing saturation in the actuators. Of course, the larger the acceleration change, the larger the nonlinear effects. To analyze if the difference is more significant for larger acceleration changes, more experiments are necessary.

VIII. Conclusions

We have generalized Incremental Nonlinear Dynamic Inversion (INDI) for the control of linear accelerations of a quadrotor subject to disturbances. The experiment in the windtunnel shows that the INDI controller better resists gusts than a traditional Proportional Integral Derivative (PID) controller. In the experiments, the quadrotor received four Hz position updates, which means that the technique can readily be applied outdoors with standard GPS modules. This is demonstrated in an outdoor experiment, where the INDI controller shows similar performance benefits as in the windtunnel. This outer loop INDI controller can increase the ability of Micro Aerial Vehicles to perform tasks that require accurate position control under gusty conditions, such as flying near obstacles, entering a building through a window, etc.

A. Future Work

The investigation of the effects of linearization in the outer loop gives rise to the question if the linearizations in the inner loop are adequately justified. A solution could be to linearly calculate increments for the inner loop, and then use the nonlinear mapping of Figure 8 to map the linear increments to the correct nonlinear increments.

Though the inner and outer loop INDI controllers are quite robust, a situation that can still lead to instability is saturation of the actuators. In this case, doing the control allocation through the inverse of the control effectiveness matrix and saturating the resultant control vector, leads to a suboptimal realization of the control objective, because some axes are more important than others. Taking the axis priorities into account when calculating the control vector might solve this problem.

Furthermore, we will apply this control method to hybrid UAVs, that combine vertical takeoff and landing with fast forward flight using a wing. These vehicles are very prone to be disturbed due to their large aerodynamic surfaces, and INDI is especially good at disturbance rejection.

Funding

This research was funded by the Delphi Consortium.

Acknowledgment

The authors would like to thank Matej Karasek, for his help with the windtunnel experiment, and Freek van Tienen, for porting the Paparazzi software to the Bebop quadrotor.

References

[1] A. Ryan and J. Hedrick, "A mode-switching path planner for UAV-assisted search and rescue," in *44th IEEE Conference on Decision and Control*, 2005, pp. 1471–1476.

[2] R. D'Andrea, "Can drones deliver?" *IEEE Transactions on Automation Science and Engineering*, vol. 11, no. 3, pp. 647–648, July 2014.

[3] J. Kim and S. Sukkarieh, "Airborne simultaneous localisation and map building," in *IEEE International Conference on Robotics and Automation*, 2003, pp. 406–411.

[4] K. Alexis, G. Nikolakopoulos, and A. Tzes, "Constrained-Control of a Quadrotor Helicopter for Trajectory Tracking under Wind-Gust Disturbances," in *IEEE Mediterranean Electrotechnical Conference*, 2010, pp. 1411–1416.

[5] M. W. Orr, S. J. Rasmussen, E. D. Karni, and W. B. Blake, "Framework for Developing and Evaluating MAV Control Algorithms in a Realistic Urban Setting," in *American Control Conference*, June 2005, pp. 4096–4101.

[6] S. Shen, N. Michael, and V. Kumar, "Autonomous Multi-Floor Indoor Navigation with a Computationally Constrained MAV," in *International Conference on Robotics and Automation*, May 2011, pp. 20–25.

[7] D. Mellinger, N. Michael, and V. Kumar, "Trajectory generation and control for precise aggressive maneuvers with quadrotors," *The International Journal of Robotics Research*, vol. 31, no. 5, pp. 664–674, 2012.

[8] N. Sydney, B. Smyth, and D. A. Paley, "Dynamic control of autonomous quadrotor flight in an estimated wind field," in *IEEE Conference on Decision and Control (CDC)*, December 2013, pp. 3609–3616.

[9] A. Mohamed, M. Abdulrahim, S. Watkins, and R. Clothier, "Development and flight testing of a turbulence mitigation system for micro air vehicles," *Journal of Field Robotics*, 2015.

[10] J. Escareño, S. Salazar, H. Romero, and R. Lozano, "Trajectory Control of a Quadrotor Subject to 2D Wind Disturbances," *Journal of Intelligent & Robotic Systems*, vol. 70, no. 1, pp. 51–63, August 2012.

[11] S. L. Waslander and C. Wang, "Wind Disturbance Estimation and Rejection for Quadrotor Position Control," in *AIAA Infotech@Aerospace Conference and AIAA Unmanned...Unlimited Conference*, April 2009.

[12] F. Schiano, J. Alonso-Mora, K. Rudin, P. Beardsley, R. Siegwart, and B. Siciliano, "Towards Estimation and Correction of Wind Effects on a Quadrotor UAV," in *International Micro Air Vehicle Conference and Competition (IMAV)*, August 2014, pp. 134–141.

[13] T. Tomić, K. Schmid, P. Lutz, A. Mathers, and S. Haddadin, "The Flying Anemometer: Unified Estimation of Wind Velocity from Aerodynamic Power and Wrenches," in *International Conference on Intelligent Robots and Systems (IROS)*, Daejeon, Korea, October 2016, pp. 1637–1644.

[14] E. J. J. Smeur, Q. P. Chu, and G. C. H. E. de Croon, "Adaptive Incremental Nonlinear Dynamic Inversion for Attitude Control of Micro Aerial Vehicles," *Journal of Guidance, Control, and Dynamics*, vol. 39, no. 3, pp. 450–461, March 2016.

[15] G. Hattenberger, M. Bronz, and M. Gorraz, "Using the Paparazzi UAV System for Scientific Research," in *International Micro Air Vehicle Conference and Competition (IMAV)*, 2014, pp. 247–252.

[16] B. Remes, D. Hensen, F. van Tienen, C. de Wagter, E. van der Horst, and G. de Croon, "Paparazzi: how to make a swarm of Parrot AR Drones fly autonomously based on GPS." in *International Micro Air Vehicle Conference and Flight Competition (IMAV)*, Toulouse, France, September 2013, pp. 307–313.

[17] E. J. J. Smeur, de G.C.H.E de Croon, and Q. Chu, "Gust disturbance alleviation with incremental nonlinear dynamic inversion," in *International Conference on Intelligent Robots and Systems (IROS)*. IEEE/RSJ, December 2016, pp. 5626–5631.

[18] G. M. Hoffmann, H. Huang, S. L. Waslander, and C. J. Tomlin, "Precision flight control for a multi-vehicle quadrotor helicopter testbed," *Control Engineering Practice*, vol. 19, no. 9, pp. 1023–1036, 2011.

[19] ——, "Quadrotor Helicopter Flight Dynamics and Control: Theory and Experiment," in *Guidance, Navigation and Control Conference and Exhibit*. AIAA Paper 2007-6461, August 2007.

[20] P. Simplicio, M. Pavel, E. van Kampen, and Q. Chu, "An acceleration measurements-based approach for helicopter nonlinear flight control using Incremental Nonlinear Dynamic Inversion," *Control Engineering Practice*, vol. 21, no. 8, pp. 1065–1077, aug 2013.

[21] J. Wang, T. Raffler, and F. Holzapfel, "Nonlinear Position Control Approaches for Quadcopters Using a Novel State Representation," in *Guidance, Navigation and Control Conference*. AIAA Paper 2012-4913, August 2012.

[22] B. J. Bacon, A. J. Ostroff, and S. M. Joshi, "Reconfigurable NDI Controller Using Inertial Sensor Failure Detection & Isolation," *IEEE Transactions On Aerospace And Electronic Systems*, vol. 37, no. 4, pp. 1373–1383, Oct 2001.

[23] E. Fresk and G. Nikolakopoulos, "Full Quaternion Based Attitude Control for a Quadrotor," in *European Control Conference*. IEEE, July 2013, pp. 3864–3869.